

Accounting for multiplicity in machine learning benchmark performance

Kajsa Møllersen¹ and Einar Holsbø²

¹Department of Community Medicine

²Department of Computer Science
UiT - The Arctic University of Norway

1 Introduction: Population vs sample state-of-the-art performance

Machine learning methods are commonly evaluated and compared by their performance on data sets from public repositories, where methods can be evaluated under identical conditions and across time. Theoretical results play an important role in machine learning research, but for the last couple of decades the success of increasingly complex methods has pushed the proof towards the pudding: performance on benchmark data sets.

The numbers don't lie: if method A performs better than method B on a specific data set, that is what it did. But the truth that the numbers tell is limited. We think of a data set, for example a collection of images, as a random sample from an underlying population. In science we are interested in the performance on the population, and the observed performance acts as an estimate. A good estimator gives a reliable result, but overfitting to the data set, originating from wrong use of cross-validation, data leakage and data reuse, can give overly optimistic estimates. An independent test set, often referred to as a hold-out set, is a sample that is not used for development of the method, and gives an unbiased estimator. Competitions and challenges with prize money typically withhold the test set so that it becomes impossible for the participants to use it for development.

Although we know these things we have a tendency to extrapolate the performance metric and interpret it as something about the world rather than something about a data set. If we always appended “on MNIST” when we said so-and-so method had accuracy so-and-so nobody would care. Who cares about MNIST? We hold out data precisely because we want to estimate some sort of long-term behavior on similar data.

An unbiased estimator solves only half of the problem; the variance tells just as much as the bias regarding the quality of a method. For machine learning methods, the sources of variance are plentiful. One is the random nature of the

test set, the training set and the validation set. In addition comes the setting of hyperparameters, which can lead to substantial variation, and minor variance sources such as random seeds and stochastic dropouts. The sources of variance that are part of the training are often referred to as influencing the method's stability or robustness. With knowledge about the behaviour of both the bias and the variance of an estimator, the error can be predicted, often in terms of a confidence interval. It is certainly more useful to know what the lower limit of the 95% confidence interval is, than the observed performance on a specific test set.

The highest ranked performance on a problem is referred to as state-of-the-art (SOTA) performance, and is used, among other things, as a reference point for publication of new methods. As a specific method's performance on a test set is just an estimate of its true underlying performance, the reported SOTA performances are estimates, and hence come with bias and variance.

State-of-the-art performance increasingly relies on benchmark data sets, often in combination with a challenge or a competition. The practice of hold-out test sets in competitions safe-guards against overoptimistic estimates for the individual classifiers. Data is often released after the competition has ended, and new methods can be compared to the state-of-the-art performance.

As we will show in the subsequent sections, using the highest-ranked performance as an estimate for state-of-the-art is a biased estimator, giving overoptimistic results. The mechanisms at play are those of multiplicity, a topic that is well-studied in the context of multiple comparisons and multiple testing, but has, as far as the authors are aware of, been nearly absent from the discussion regarding state-of-the-art estimates.

Biased state-of-the-art has consequences both for practical implementations and for research itself. A health care provider might want to use some machine learning method for tumour detection, but only if the method correctly classifies at least 80%. The health care provider closely follows updates on state-of-the-art performance, and are ready to invest time and money in a pilot project once the lower bound surpasses 80%. If the state-of-the-art performance is an optimistic estimate, the health care provider has now lost time and money, and perhaps also some faith in research results.

For the research community, the situation is perhaps even more dramatic. The optimistic state-of-the-art estimate is used as a standard for evaluating new methods. Not to say that a new method necessarily needs to beat the current state-of-the-art to catch interest from reviewers and editors, but it certainly helps if its performance is comparable. It has been pointed out (see Section 2) that the incremental increase in performance can obstruct the spread of new ideas that have substantial potential, but just haven't reached their peak yet.

In this article, we provide a probability distribution for the case of multiple classifiers. We demonstrate the impact of multiplicity through simulated examples. We show how classifier dependency impacts the variance, but also that the impact is limited when the accuracy is high. Finally, we discuss a real-world example; a Kaggle competition from 2020. All code is available at <https://github.com/3inar/ninety-nine>.

2 Related work

Multiple comparisons is a well-studied subject within statistics, see, e.g., Tukey [1991] for an interesting discussion on some topics of multiple comparisons, among them the confidence intervals. For a direct demonstration of how multiple testing can lead to false discoveries, Bennett et al. [2009] gives an example where brain activity is detected in a (dead) salmon “looking” at photos of people. In the machine learning context, with multiple data sets and classifiers, Demšar [2006] suggests adjusting for multiple testing, according to well-known statistical theory. Our article focuses on the estimate itself and its uncertainty, and not comparison of methods.

The re-use of benchmark datasets has been addressed in several publications. Salzberg [1997] point to the problem that arises because these datasets are static, and therefore run the risk of being exhausted by overfitting. Exhausted public data sets still serve important functions, e.g., a new idea can show to perform satisfactory, even when it is not superior. Thompson et al. [2020] distinguishing between simultaneous and sequential multiple correction procedures. In sequential testing, which is the reality of public datasets, the number of tests is constantly updated. An interesting topic they bring up is the conflict between sharing incentive, open access and stable false positive rate. There are several demonstrations of the vulnerability of re-use of benchmark datasets. Teney et al. [2020] performed a successful attack on the VQA-CP benchmark dataset, that is, they are able to attain high performance with a non-generalisable classifier. They point towards the risk of ML methods capturing idiosyncrasies of a dataset. Torralba and Efros [2011] introduced the game Name That Dataset! motivating their concern of methods being tailored to a dataset rather than a problem. The lack of statistically significant differences among top performing methods is demonstrated by, e.g., Everingham et al. [2015] and Fernández-Delgado et al. [2014].

The same mechanisms of overfitting are present in challenges through multiple submissions to the validation set. Blum and Hardt [2015] introduced an algorithm that releases the public leaderboard score only if there has been significant improvement compared to the previous submission. This will prevent overfitting by hindering adjustments to random fluctuations in the score, and not true improvements of the method. Dwork et al. [2017] use the principles of differential privacy to prevent overfitting to the validation set.

Several publications show that the overfitting is not as bad as expected, and provide possible explanations. Recht et al. [2019] constructed new, independent test sets of CIFAR-10 and ImageNet. They found that the accuracy drop is dramatic, around 10%. However, the order of the best performing methods is preserved, which can be explained by the fact that multiple classes (Feldman et al. [2019]) and model similarity (Mania et al. [2019]) slows down overfitting. Roelofs et al. [2019] compared the results from the private leaderboard (one submission per team) and the public leaderboard (several submissions per team) in Kaggle challenges. Several of their analyses indicate overfitting even though their main conclusion is that there is little evidence of overfitting.

Overfitting and its consequences are avoided in most challenges by withholding the test set so that a method can only be evaluated once and not adapted to the test set performance. Hold-out datasets also prevents wrong use of cross-validation, see, e.g., Fernández-Delgado et al. [2014] and the seminal paper of Dietterich [1998]. Another contribution from public challenges is the requirement of reproducibility to collect the prize money, which is a well-known concern in science, see, e.g., Gundersen and Kjensmo [2018]. Public challenges typically rank the participants by a (single) performance measure, and can fall victims of Goodhart’s law, paraphrased as “When a measure becomes a target, it ceases to be a good measure.” by Teney et al. [2020]. Ma et al. [2021] offers a framework and platform for evaluation of NLP methods, where other aspects such as memory use and robustness are evaluated.

The robustness/stability of a method, and the variability in performance are crucial aspects that the hold-out test set of public challenges does not offer an immediate solution to. Bouthillier et al. [2021] showed empirically that hyperparameter choice and the random nature of the data are two large contributors to variance, whereas data augmentation, dropouts, and weights initialisations are minor contributors. Choice of hyperparameters are often adjusted to validation set results, and the strategies of Blum and Hardt [2015] and Dwork et al. [2017] can hinder that, if implemented by the challenge hosts. Our contribution is a focus on better estimate for state-of-the-art performance under the current conditions, where the approach of Bouthillier et al. [2021] does not apply. Bousquet and Elisseeff [2002] investigate how sampling randomness influences accuracy, both for regression algorithms and classification algorithms, relying on the work of Talagrand [1996] who stated that “A random variable that depends (in a “smooth” way) on the influence of many independent variables (but not too much of any of them) is essentially constant.”

There is a rich literature on various aspects regarding the use of public challenges as standards for scientific publications, see, e.g., Varoquaux and Cheplygina [2022] for a much broader overview than the one given here. Concerns and solutions regarding multiplicity and better performance estimates are active research fields. We contribute to this conversation by shining the light on how multiplicity of classifiers’ performance on hold-out test sets create optimistic estimates of state-of-the-art performance.

3 Multiple classifiers and biased state-of-the-art estimation

3.1 Notation

- n : number of trials/size of test set
- θ : probability of success/probability of correct prediction
- m : number of experiments/number of classifiers
- $\mathcal{B}ern(\theta)$: Bernoulli distribution
- Y : random variable, indicates if prediction is correct
- $Y \sim \mathcal{B}ern(\theta)$
- $\mathcal{B}(n, \theta)$: binomial distribution
- X : random variable, number of failures in one experiment
- $X \sim \mathcal{B}(n, 1-\theta)$
- $\hat{\theta}(X) = \frac{n - X}{n}$: estimator for θ , unbiased
- $P(X = x)$: probability of x failures in one experiment
- $P_x = P(X \leq x)$: probability of at most x failures in one experiment
- $\mathbf{X} = \{X_1, X_2, \dots, X_m\}$: random sample, number of failures for classifiers $j = 1, \dots, m$
- C_x : random variable, number of experiments with at most x failures
- $C_x \sim \mathcal{B}(m, P_x)$
- Z : random variable, the smallest number of failures among all classifiers
- θ_{SOTA} : highest probability of correct prediction among all classifiers
- $\hat{\theta}_{SOTA}^{max}(\mathbf{X}) = \max_j \hat{\theta}_j$: estimator for θ_{SOTA} , biased
- α : significance level

3.2 Two coin-flip examples

Multiplicity is, simply put, how the probability of an outcome changes when an experiment is performed multiple times. Consider $n = 20$ flips of a fair coin where the outcome is the number of heads, referred to as the number of successes in a binomial distribution, $\mathcal{B}(n, \theta)$, where the probability of success is $\theta = 0.5$. Let the random variable X denote the number of failures, $X \sim \mathcal{B}(n, 1-\theta)$. The probability of 15 heads or more corresponds to observing $x = n - 15$ tails or less, that is, the cumulative distribution $P(X \leq x|n, 1-\theta)$. This corresponds to the cumulative distribution for the estimator $\hat{\theta}(X) = \frac{n-X}{n}$, and we have that $P(\hat{\theta}(X) \geq \frac{n-x}{n}) = P(X \leq x) = 0.02069$ for $\hat{\theta} \geq 0.75$. In other words, if $\theta = 0.5$, there is a probability of 0.02069 that the estimate is 0.75 or above in a series of $n = 20$ trials. The probability of exactly $x = 5$ can be calculated from the probability mass function (pmf) $P(X = x|n, 1-\theta) = 0.01479$, but the interest

usually lies with the cumulative distribution. We focus on the case where $X \leq x$, but it is straightforward to substitute $P(X \leq x)$ for $P(X = x)$ in the following.

If we fix x we can define the experiment described above as a Bernoulli trial, where success is defined as $X \leq x$, with corresponding probability $P(X \leq x)$, which we from now on write as P_x for ease of notation. If we perform the coin-flip experiment m times, and success is defined as $X \leq x$, we have a series of m Bernoulli trials, and the number of successes follow the binomial distribution $\mathcal{B}(m, P_x)$. Let C_x be the random variable that denotes the number of successful experiments. The probability of, for example, $C_x = 10$ experiments with at most $x = 5$ tails, is calculated from the pmf $P(C_x = 10|m, P_x)$. Of special interest is the case where at least one experiment succeeds, $P(C_x > 0) = 1 - P(C_x = 0)$. In our example, if the coin-flip experiment is performed $m = 100$ times, the probability of observing 15 heads or more at least once is $P(C_x > 0|m, P_x) = 1 - P(C_x = 0|m, P_x)$, with $P_x = 0.02069$ from above. In the estimation context, we have that although the probability of $\hat{\theta} \geq 0.75$ is only 0.02069 for the individual experiments, the probability of at least one $\hat{\theta} \geq 0.75$ is 0.8765 when the experiment is performed $m = 100$ times.

Consider an experiment where a coin is flipped $n = 20$ times, and the number of successes is the number of times a classifier correctly predicts the outcome. An unbiased estimator for a classifier’s probability of correct prediction, θ , is $\hat{\theta} = (n - X)/n$, where X is the number of failures. The corresponding estimate is referred to as accuracy. The true state-of-the-art for coin-flip classifiers is $\theta_{SOTA} = 0.5$, since it is impossible to train a classifier to predict coin flips. If $m = 1,000$ classifiers independently give their predictions for $n = 20$ flips, we can consider this as a binomial experiment with 1,000 Bernoulli trials, where the probability of success is the individual classifier’s probability of $n - X \leq n - x$ correct predictions. The probability of at least one classifier achieving an accuracy of at least 0.90 is $1 - P(C_x = 0|m, P_x) = 0.1823$, where $P_x = P(X \leq 18|n, 1-\theta) = 0.00020$. This means that using the top-ranked method as an estimate and ignoring multiplicity there is a substantial risk of overestimating the state-of-the-art.

3.3 The probability distribution of $\hat{\theta}_{SOTA}^{max}$

We define the SOTA probability of correct prediction, θ_{SOTA} , as the highest probability of correct prediction among all classifiers *applied to a test set*, in accordance with the common set-up for public competition. Of interest is $P(\hat{\theta}_{SOTA}^{max}|m, n, \theta)$, the probability of $\hat{\theta}_{SOTA}^{max}$, being the estimated state of the art from taking the highest ranked classifier, given the number of classifiers, the size of the test set, and the probabilities of correct prediction, $\theta = \{\theta_1, \dots, \theta_m\}$.

We will in the following assume independent classifiers, and discuss dependency in Section 4. We demonstrate the impact of multiplicity in the simple case of identical probabilities of correct prediction, $\theta_j = \theta$ for all classifiers, $j = 1, \dots, m$, and where $\theta_{SOTA} = \theta$. We discuss non-identical probabilities in Section 4.2.

Let n denote the size of the test set, m be the number of classifiers, and

θ be the probability of correct prediction. Let X be the random variable that denotes the number of failures (wrong predictions) for a given classifier. We have that $X \sim \mathcal{B}(n, 1-\theta)$. We denote by P_x the cumulative distribution $P(X \leq x)$. The random sample, $\mathbf{X} = \{X_1, X_2, \dots, X_m\}$ consists of the number of wrong predictions for each classifier $j = 1, \dots, m$ on a test set. Let C_x be the random variable that denotes the number of classifiers with at most x failures. We have that $C_x \sim \mathcal{B}(m, P_x)$, because each classifier will independently have a probability P_x of having at most x wrong predictions.

We are interested in the probability of at least one classifier having at most x wrong predictions, because it corresponds to the probability function of the $\hat{\theta}_{SOTA}^{max}$ estimator, $P(\hat{\theta}_{SOTA}^{max} > \frac{n-x}{n})$, in other words, at least one $\hat{\theta}_j > \frac{n-x}{n}$. We can derive this from C_x :

$$P(C_x > 0 | m, n, \theta). \quad (1)$$

Note that this corresponds to the cumulative distribution function (cdf) $F(z)$ for the random variable Z , denoting the most wrong predictions among all classifier. We have cdf $F(z)$, the probability that the most wrong predictions among all classifiers is less than or equal to a number z , can easily be derived from the binomial distribution

$$\begin{aligned} F(z) &= P(C_z > 0 | m, n, \theta) = 1 - P(C_z = 0 | m, P_z) \\ &= 1 - (1 - P_z)^m. \end{aligned} \quad (2)$$

Let $f(z)$ denote the probability mass function of Z . We then have

$$\begin{aligned} f(z) &= F(z) - F(z-1) = 1 - (1 - P_z)^m - \{1 - (1 - P_{z-1})^m\} \\ &= (1 - P_{z-1})^m - (1 - P_z)^m = \\ &= (1 - \sum_{\ell=0}^{z-1} P(Z = \ell))^m - (1 - \sum_{\ell=0}^{z-1} P(Z = \ell) - P(Z = z))^m \\ &= - \sum_{k=1}^m (-1)^k \binom{m}{k} (1 - \sum_{\ell=0}^{z-1} P(Z = \ell))^{m-k} P(Z = z)^k. \end{aligned} \quad (3)$$

The last line is derived by binomial expansion. The practical relevance of the binomial expansion is limited by the need to approximate binomial coefficient for large m . From Eq. 3, the expected value and variance can easily be calculated. An example of $F(z)$ can be seen in Fig. 2, and the corresponding $f(z)$ in Fig. 3. The pmf $f(z) = P(Z = z)$ denotes the probability of at least one classifier having exactly z wrong predictions, and no classifiers having fewer than z wrong predictions.

3.4 A simulated public competition example

The multiplicity mechanisms described above apply to public competitions where several teams submit their predictions on a test set. Winning teams are those

with highest accuracy, $\max_j \hat{\theta}_j$, where $\hat{\theta}_j = (n - x_j)/n$ is the accuracy of a classifier j on the test set. This is often referred to as the state of the art, and hence, we have that $\hat{\theta}_{SOTA}^{max}(\mathbf{x}) = \max_j \hat{\theta}_j$. As exemplified in Section 3.2, multiplicity biases the estimation of θ_{SOTA} , and Section 3.3 gives us the tools to analyze its impact. In the following, we will use a significance level of $\alpha = 0.05$ and two-sided confidence intervals.

Consider a classification problem with a test set of size $n = 3,000$, and a classifier with probability of correct prediction $\theta = 0.90$. The pmf of a single classifier is shown as a histogram in Fig. 1. The 95% confidence interval for θ if we have observed $\hat{\theta} = 0.90$ is $(0.8887, 0.9105)$, and we denote it by $(\theta_{\alpha/2}, \theta_{1-\alpha/2})$.

If there are $m = 1,000$ classifiers, each with probability of correct prediction $\theta = 0.90$, the probability of at least one team achieving at least $\theta_{1-\alpha/2}$ is close to 1. This comes as no surprise given the definition of a confidence interval. It means that we can be almost certain that the accuracy of the top ranked classifier, which is the default SOTA, is above the upper limit of the confidence interval of the true performance.

On the other hand, it is straightforward to show that if each individual classifier has a probability of $P_x = 0.00002532$ for at most x failures, then, with a probability of $\alpha/2$, at least one team will achieve at least $\hat{\theta} = 0.9213$. We denote this by $\theta_{1-\alpha/2}^m$, the multiplicity-adjusted upper limit of the $(1-\alpha)$ confidence interval.

Similarly, the expected value of $\hat{\theta}_{SOTA}^{max}$ can easily be calculated from Eq. 3, and we have $E(\hat{\theta}_{SOTA}^{max}) = 0.9173$. Both are optimistic estimates, knowing that θ_{SOTA} is 0.90.

Within the competition context, this is not necessarily a problem, because each team has the same probability of achieving the highest accuracy given that they have the same θ . In a scientific context, using $\max_j \hat{\theta}_j$ as an estimate for θ_{SOTA} without multiplicity corrections is problematic. Consider a new classifier with probability of correct prediction $\theta_{m+1} = \theta_{1-\alpha/2}$ from above, displayed as the red curve in Fig. 1. By common scientific standards, the expected performance, $E(\hat{\theta}_{m+1}) = \theta_{m+1}$ is considered significantly better than the expected performance of any of the 1,000 classifiers with $\theta = 0.90$, and is of interest to the research community. But the probability of this classifier beating the upper limit of the multiplicity adjusted confidence interval is very low: $P(\hat{\theta}_{m+1} \geq \theta_{1-\alpha/2}^m) = 0.0190$, and can be seen as the red area in Fig. 1. Similarly, $P(\hat{\theta}_{m+1} \geq E(\hat{\theta}_{SOTA}^{max})) = 0.0996$, seen as the blue plus red area in Fig. 1. This means that by using the maximum accuracy as SOTA, we can expect that 9 out of 10 classifiers that are in fact better will still be naively considered worse.

The cumulative distribution function, $F(z)$ from Eq. 2, is displayed in Fig. 2, and describes the cumulative probability of at least one classifier having at most z failures. Or, in other words, the cumulative probability of maximum accuracy. The number of failures are displayed on the top horizontal axis, and the corresponding accuracy on the bottom horizontal axis. Note that the horizontal axis is reversed compared to Fig. 1. The corresponding pmf, $f(z)$ from Eq. 3, is displayed as a histogram in Fig. 3.

The probability mass functions of single $\hat{\theta}$.

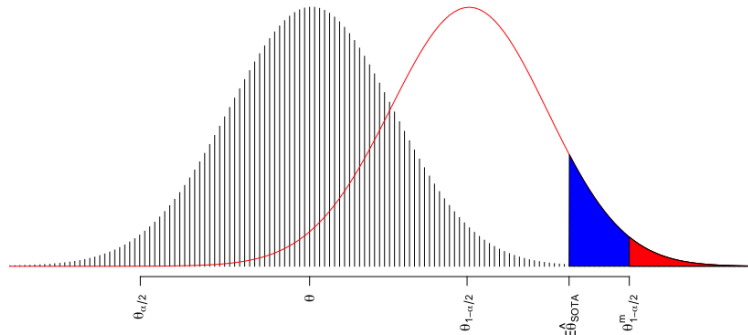


Figure 1: The grey histogram shows the pmf of a classifier with probability of correct prediction θ . The red curve is the pmf of a classifier with probability of correct prediction $\theta_{1-\alpha/2}$, the upper limit of the 95% CI for $\hat{\theta}(\mathbf{x}) = \theta$. $E(\hat{\theta}_{SOTA}^{max})$ denotes the expected value of the highest ranked among $m = 1,000$ classifiers. $\theta_{1-\alpha/2}^m$ is the multiplicity corrected upper limit of the 95% CI. The shaded areas corresponds to $P(\hat{\theta}_{m+1} \geq \theta_{1-\alpha/2}^m)$ (red) and $P(\hat{\theta}_{m+1} \geq E(\hat{\theta}_{SOTA}^{max}))$ (blue+red).

Cumulative distribution function, $F(z|m, n, \theta)$, for at least one classifier having at most z failures.

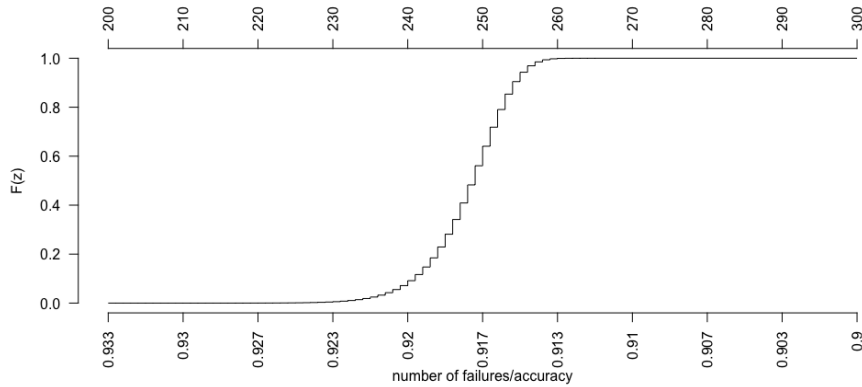


Figure 2: The figure shows the cumulative distribution function for at least one classifier having at most z failures. The horizontal axis denotes the number of failures, z , on top and the accuracy at the bottom.

Probability mass function, $f(z|m, n, \theta)$, for the smallest number of failures, z , among all classifiers.

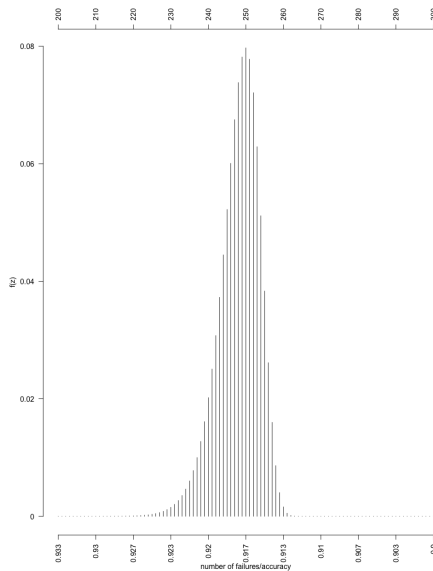


Figure 3: The figure shows the corresponding pmf for Fig. 2. The horizontal axis denotes the number of failures, z , on top and the corresponding accuracy at the bottom.

From Eq. 3 we get the expected value and variance. For $m = 1,000$, $n = 3,000$ and $\theta = 0.9$ this corresponds to $E(\hat{\theta}_{SOTA}^{max}) = 0.9173$ with a standard deviation of 0.001817. We can see how different values for m , n and θ affects the $\hat{\theta}_{SOTA}^{max}$ distribution in Table 1.

Expected values and standard deviations for $\hat{\theta}_{SOTA}^{max}$

m	n	θ	$E(\hat{\theta}_{SOTA}^{max})$	$\sigma_{\hat{\theta}_{SOTA}^{max}}$
1,000	3,000	0.85	0.8707	0.002197
1,000	3,000	0.90	0.9173	0.001817
1,000	3,000	0.95	0.9624	0.001277
100	3,000	0.90	0.9135	0.002250
500	3,000	0.90	0.9163	0.001923
1,000	1,000	0.90	0.9294	0.003007
1,000	10,000	0.90	0.9096	0.001022

Table 1: The expectation and standard deviation for the SOTA estimator with varying test set size, number of classifiers and probability of correct prediction. The bold line is the example used in Fig. 3.

4 Non-i.i.d.

The probability distribution in Section 3.4 is based on independent classifiers with identical θ s. This assumption is rarely true in practice. A classifier’s ability to perform better than random guesses is due to correlation between features and labels in a training set. The teams will pick up on many of the same features and correlations, regardless of which method they choose. In addition, many teams will use different versions of related methods. We investigate dependency and non-identical classifiers, and the impact on the bias. Table 2 gives an overview, details are in the following sections.

Upper bounds, expected values and standard deviations for $\hat{\theta}_{SOTA}^{max}$

section	independent	identical	upper 95% CI	expected value	standard deviation
3.4	YES	YES	0.9213	0.9173	0.001817
4.1	NO	YES	0.9207	0.9140	0.003481
4.1	NO*	YES	0.9173	0.9140	0.001484
4.2	YES	NO	0.9177	0.9130	0.002129
4.3	NO	NO	0.9173	0.9101	0.003649

Table 2: The upper bound of the 95% CI, the expectation and standard deviation for the SOTA estimator for different combinations of independency and identity. The true state-of-the-art is $\theta = 0.90$.

4.1 Dependent, identical classifiers

Let Y_j be the Bernoulli variable with value 1 if classifier j predicts a data point correctly. We have $P(Y_j = 1) = \theta_j$, and $\theta_j = \theta$ for classifiers with equal probability of success. Mania et al. [2019] calculated the similarity, defined as the fraction of two models giving the same output, which is equivalent to

$$\begin{aligned} P(\{Y_j, Y_k\} = \{0, 0\}) + P(\{Y_j, Y_k\} = \{1, 1\}) \\ = (1 - \theta_j)(1 - \theta_k) + \theta_j\theta_k \end{aligned} \quad (4)$$

for independent models. For dependent models with correlation ρ_{jk} , this becomes

$$(1 - \theta_j)(1 - \theta_k) + \theta_j\theta_k + 2\rho_{jk}\sqrt{\theta_j\theta_k(1 - \theta_j)(1 - \theta_k)}. \quad (5)$$

By setting $\theta_j = \theta$ and $\rho_{jk} = \rho$, ρ can easily be estimated from the estimations of θ , $P(\{Y_j, Y_k\} = \{0, 0\})$ and $P(\{Y_j, Y_k\} = \{1, 1\})$. In Mania et al. [2019], they used the average accuracy for top-performing ImageNet models, $\hat{\theta} = 0.756$. For details, see Mania et al. [2019]. Note that these are multi-class problems, so a lower accuracy than for binary classification problems is to be expected. From their calculated similarity of 0.85, the estimated correlation is 0.36.

Boland et al. [1989] describes dependency in the majority systems context, with $\rho_{0j} = \text{corr}(Y_0, Y_j)$, $j = 1, \dots, m$, and the Y_j s are independent given Y_0 . This gives $\rho_{jk} = \rho_{0j}^2$. The observations from Y_0 does not contribute directly to $\hat{\theta}_{SOTA}^{max}$, but can be seen as, e.g., the influence that a common training set has on the classifiers.

The binomial distribution for dependent Bernoulli trials is not an easy problem, see, e.g., Ladd [1975] and Hisakado et al. [2006]. We here demonstrate by simulation how dependency reduces the bias. We use the estimated correlation from Mania et al. [2019], which corresponds to $\rho_{0j} = 0.6$ in the multiplicity set-up with an external Y_0 .

We use the set-up from Section 3.4 with $m = 1,000$ classifiers, test set size $n = 3,000$, and probability of correct prediction $\theta = 0.90$. We simulate two scenarios; one where Y_0 is random, and one where the y_0 's are fixed with exactly $(n - x)/n = 0.90$ correct predictions. The fixed scenario can correspond to fixed training conditions, e.g., models pre-trained on ImageNet. The random scenario picks up the randomness in, e.g., a training set. Although all teams have the same training set, the training set is a random sample.

The upper bound of the 95% confidence interval for the dependent classifiers is at 0.9173 for the fixed y_0 and 0.9207 for the random Y_0 , but they have the same expected value.

Minimum number of failures in $m = 1,000$ classifiers.

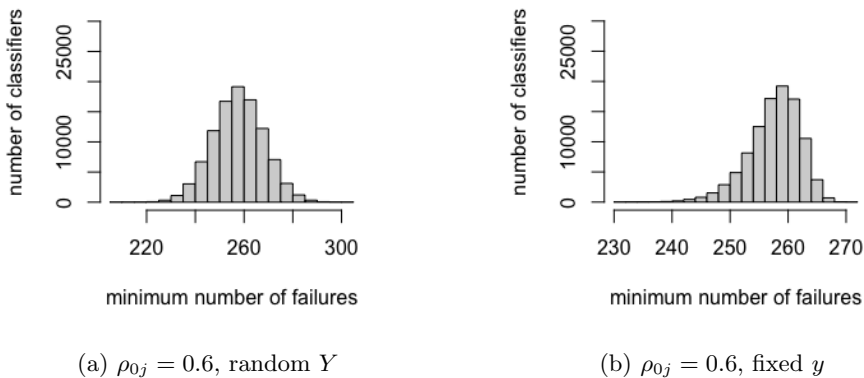


Figure 4: The minimum number of failures in 100,000 simulations, with probability of success $\theta = 0.9$.

Note that, with $\theta = 0.90$, the similarity as described by Mania et al. [2019] is 0.82 for two independent classifiers. When the probability of correct prediction is high, there is little room for variation between classifiers, and the inherent similarity is high.

4.2 Non-identical, independent classifiers

The Poisson Binomial distribution, see, e.g., Wang [1993], describes the sum of n non-identical independent Bernoulli trials with success probabilities p_1, p_2, \dots, p_n . The pmf for K number of successes is

$$P(K = k) = \sum_{A \in G_k} \prod_{i \in A} p_i \prod_{j \in A^c} (1 - p_j), \quad (6)$$

where G_k is all subsets that can be selected from $\{1, 2, \dots, n\}$.

In the multiple classifier context, we are interested in generalising Eq. 2 to the non-identical case.

$$F(z) = P(C_z > 0 | m, n, \theta) = 1 - P(C_z = 0 | m, n, \theta), \quad (7)$$

where $P(C_z = 0)$ corresponds to 0 classifiers with non-identical probabilities of success, $P(Z \leq z | \theta_j)$. The cdf is

$$\begin{aligned} F(z) &= 1 - \sum_{A \in G_0} \prod_{i \in A} P(Z \leq z | \theta_i) \prod_{j \in A^c} (1 - P(Z \leq z | \theta_j)) \\ &= 1 - \prod_{j=1}^m (1 - P(Z \leq z | \theta_j)). \end{aligned} \quad (8)$$

The pmf is

$$\begin{aligned} f(z) &= F(z) - F(z-1) \\ &= 1 - \prod_{j=1}^m (1 - P(Z \leq z | \theta_j)) - \{1 - \prod_{j=1}^m (1 - P(Z \leq z-1 | \theta_j))\} \\ &= \prod_{j=1}^m (1 - P(Z \leq z-1 | \theta_j)) - \prod_{j=1}^m (1 - P(Z \leq z | \theta_j)) \\ &= \prod_{j=1}^m \left(1 - \sum_{k=0}^{z-1} \binom{n}{k} (1 - \theta_j)^k \theta_j^{n-k}\right) - \prod_{j=1}^m \left(1 - \sum_{k=0}^z \binom{n}{k} (1 - \theta_j)^k \theta_j^{n-k}\right) \end{aligned} \quad (9)$$

Analytically, it is more complex than the case of identical classifiers, but it is easy to simulate.

We use a similar set-up as in Section 3.4 with $m = 1,000$ classifiers, test set size $n = 3,000$, and probabilities of correct prediction $\theta = \{\theta_1, \dots, \theta_m\}$, where $\min \theta = 0.875$, $\max \theta = 0.90$, and they are equally spaced.

The simulated non-identical upper bound of the 95% confidence interval is 0.9177, with 100,000 repetitions. The $E(\hat{\theta}_{SOTA}^{max})$ is 0.9129, with standard deviation of 0.0021. The cdf and pmf are displayed in Fig. 5 and Fig. 6.

4.3 Non-identical, dependent classifiers

The most complex, but also the most realistic case, is where classifiers are non-identical and dependent. An analytical solution is not known Hisakado et al.

Cumulative distribution function for non-identical classifiers.

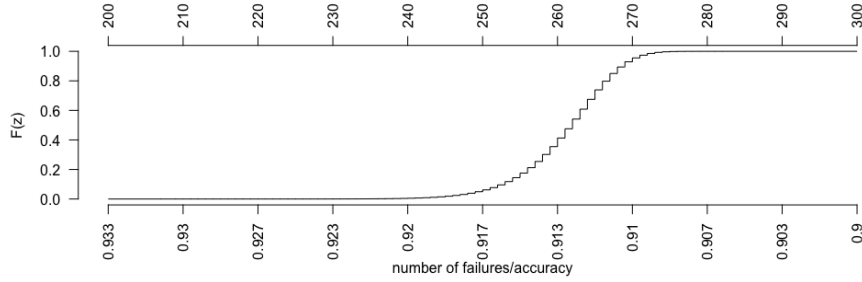


Figure 5

Probability mass function for non-identical classifiers.

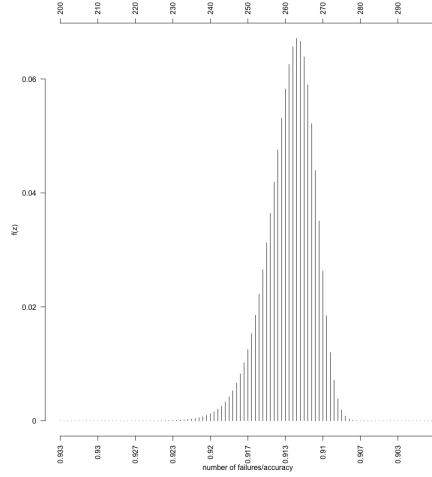


Figure 6

[2006], but simulations are easy. The results of Boland et al. [1989] are easily extended, and we have that

$$P(Y_j|Y_0 = 1) = \frac{\rho\sqrt{\theta_j(1-\theta_j)\theta_0(1-\theta_0)} + \theta_j\theta_0}{\theta_0} \quad (10)$$

$$P(Y_j|Y_0 = 0) = \frac{-\rho\sqrt{\theta_j(1-\theta_j)\theta_0(1-\theta_0)} + \theta_j(1-\theta_0)}{(1-\theta_0)}. \quad (11)$$

Note that, since $P \leq 1$, it follows from 11 that

$$\theta_j \geq \frac{\rho^2 \frac{\theta_0}{1-\theta_0}}{1 + \rho^2 \frac{\theta_0}{1-\theta_0}}, \quad (12)$$

and similarly for $0 \leq P$ and 10.

We get the a the simulated dependent upper bound of the 0.95 confidence interval of 0.91733, with 100,000 repetitions.

5 Real world examples

As we have shown above with simulated data, the observed maximum is an overoptimistic estimate for SOTA. These results are based on known state-of-the-art, but faced with real world data, the problem to be solved is of opposite nature: The observed $\hat{\theta}^{max}$ is known, but the true SOTA must be estimated. In the public competition or public data set context there are many factors that come in to play, making the bias calculations everything but straightforward.

We here demonstrate different aspects of real world analysis through SOTA estimation of three different cases: Obesity Risk (5.1.1), Cassava Leaf (5.1.2, and Melanoma (5.2). Obesity Risk and Cassava Leaf have accuracy, defined as $\hat{\theta}$, as their ranking criterion, whereas Melanoma has area under the receiver operating characteristic (ROC) curve (AUC) as ranking criterion. To estimate multiplicity effect on the AUC scores is not as straightforward as with accuracy, but the mechanisms are the same and AUC is a more common ranking criterion than accuracy.

In a public competition with m participating teams, let $\hat{\theta}_j$, $j = 1, \dots, m$ be the estimated probability of correct prediction for each classifier based on the performance on an independent test set of size n . We will refer to these as the competition observations. $\hat{\theta}^{max}$ is the observed performance of the winning team. Among the different scenarios presented in Section 4, the non-identical dependent is the most realistic model. Whereas in Table 2 we simulated $E(\hat{\theta}^{max})$ from known $\theta_1, \dots, \theta_m$, the task is now to estimate θ_{SOTA} based on $\hat{\theta}_1, \dots, \hat{\theta}_m$. A 'natural' approach is to find $\tilde{\theta}_1, \dots, \tilde{\theta}_m$ that gives $E(\hat{\theta}^{max}) = \hat{\theta}^{max}$. That is, find a set of θ 's so that the expected value of the observed maximum on a test set of size n is equal to the competition observed maximum. We use a straightforward set-up, where the simulated $\hat{\theta}_j$ is the mean value of n realisations of Y_j , where $P(Y_j) = \tilde{\theta}_j$. The simulation is repeated 10,000 times, and for each repetition the observed maximum value is recorded. $E(\hat{\theta}^{max})$ is the mean value over the repetitions.

In the studies in Section 4, the $\theta_1, \dots, \theta_m$ were chosen to be equally spaced, but this does not align with the competition observations, as seen in Figures 7a, 8a and 9. We base our suggested $\tilde{\theta}_j$'s on cropping the competition observations, as seen, e.g., in Figure 7c, but this is far from the only approach. Shrinking, which we also investigated, might give a more realistic set of $\tilde{\theta}_j$'s, but it also requires an extra parameter. For the examples presented here shrinking gave similar results to cropping, and are therefore not included.

An alternative to the expected value of the observed maximum is the upper limit of the 95% CI. The latter is more in line with common interpretation of the uncertainty of observed results for research, but which to choose will

depend on the aim of the analysis. We demonstrate the impact in the Obesity Risk example, reported in Table 3.

Not every $\hat{\theta}^{max}$ is a result of multiplicity, and we demonstrate this in the Cassava Leaf example.

5.1 Estimating θ_{SOTA}

5.1.1 Multi-Class Prediction of Obesity Risk

Multi-Class Prediction of Obesity Risk is a competition in the 2024 Kaggle Playground Series, using a synthetic data set generated from the *Obesity or CVD risk* data set (10.34740/kaggle/dsv/7009925). The test set size was $n = 13,840$, and the number of participating teams were $m = 3,498$ (excluding teams with accuracy lower than chance). The best performing team had $\hat{\theta}^{max} = 0.9116$. Figure 7a shows the competition observations, $\hat{\theta}_j$'s, zoomed in at the 3,081 best performing teams. The 95% (not multiplicity-corrected) CI for $\hat{\theta}^{max}$ is (0.9067, 0.9162) and is shown as the red line in Figure 7a, the lower bound enveloping 920 of the competition observations. This should raise suspicion that the right tail seen in Figure 7a can be the product of multiplicity.

To demonstrate the impact of ignoring multiplicity, let $\tilde{\theta}_1, \dots, \tilde{\theta}_m$ be equal to the competition observations and calculate the expectation of the maximum value of a realisation. We use the set-up from Section 4.3 with correlation coefficient $\rho = 0.6$, and random Y_0 with $\theta_0 = \hat{\theta}^{max}$. Note that competition observations with low values are excluded in accordance with Eq. 12, but they are not influencing the maximum.

A realisation is shown in Figure 7b. The upper tail, whose tip represents the maximum observed value, is stretched according to the variances of the Y_j s.

The estimated expected maximum is $E(\hat{\theta}^{max}) = 0.9159$, far above the observed maximum. The 95% CI is calculated by $B = 1,000$ bootstrap samples of size m drawn from the competition observations, and then the simulation as described above is conducted for each bootstrap sample. The values are reported in Table 3. The lower bound exceeds $\hat{\theta}^{max}$, and we can conclude that the maximum observed value is an unlikely candidate for state-of-the-art.

Perhaps a more interesting problem is finding a set $\tilde{\theta}_1, \dots, \tilde{\theta}_m$ that can result in realisations similar to the competition observations in terms of maximum observed value, and let the maximum $\tilde{\theta}_j$ be the state-of-the-art candidate.

To obtain a set $\tilde{\theta}_1, \dots, \tilde{\theta}_m$ where the expected maximum is the same as the maximum of the competition observations, $E(\hat{\theta}^{max}) = \hat{\theta}^{max}$, we crop the competition observations, as seen in Figure 7c, and where $E(\hat{\theta}^{max})$ is calculated from simulations as described above. Figure 7d shows one realisation of the cropped distribution, where the maximum observed value is close to $\hat{\theta}^{max}$. By cropping at 0.9062 we obtain $E(\hat{\theta}^{max}) = \hat{\theta}^{max}$, and this serves as a new candidate for the state-of-the-art.

It can be argued that the new SOTA candidate is at risk of being a optimistic estimate, since the competition observations are from only one test set.

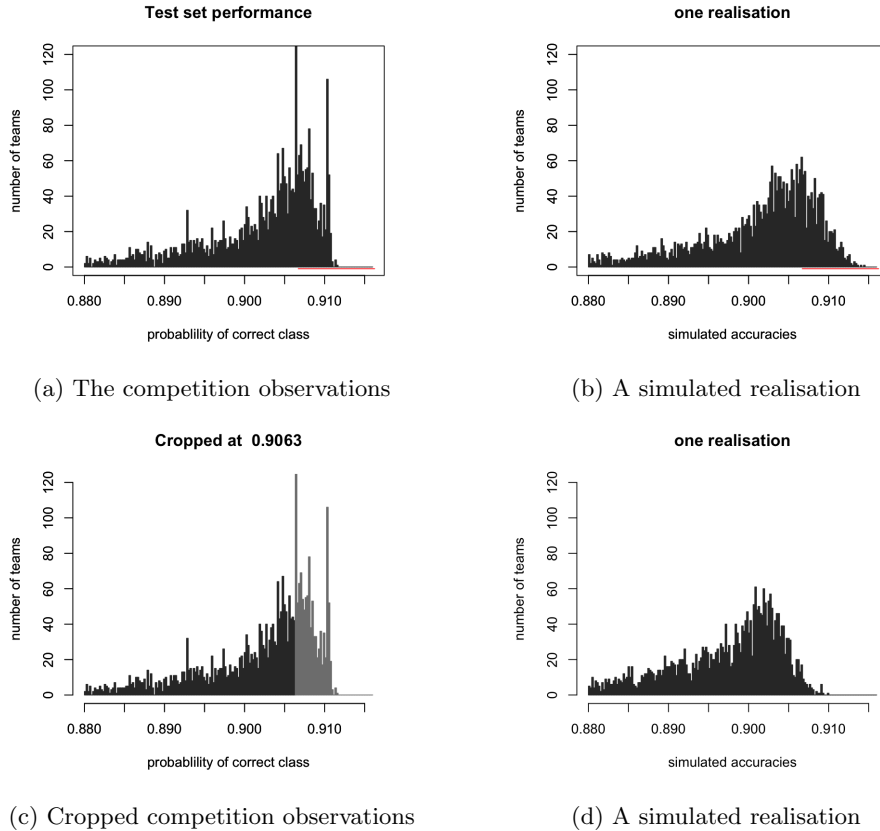


Figure 7: The competition observations and simulated realisation of classifiers with corresponding probabilities of correct classification. The red line is the 95% CI for $\hat{\theta}^{\max}$ in (a).

The upper bound of the 95% CI can mitigate such a risk, and the competition observations are cropped to fit that criterion. The CI is calculated by bootstrapping, as described above. The results are shown in Table 3.

Table 3 demonstrates that taking the effect of multiplicity into account changes how results are perceived dramatically. A more likely SOTA value is 0.9062, and even though its reduction from best performance is only about 0.005, the effect it has on who we consider performing at SOTA-level is dramatic: around one third of the teams have observed performance above the new SOTA. The more conservative approach using the upper bound of the 95% CI to estimate SOTA gives an even more dramatic result, and either way the impact is substantial.

Estimating θ_{SOTA}

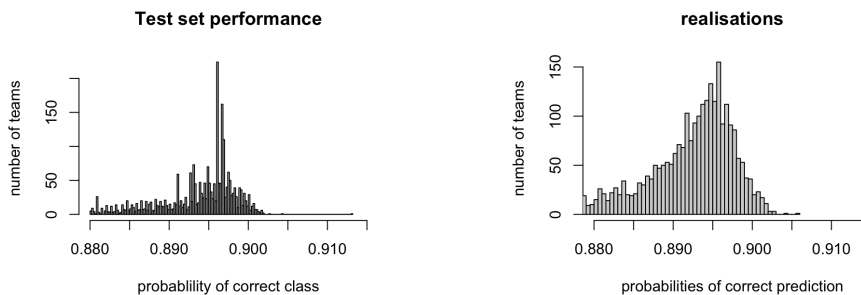
Approach	$\hat{\theta}_{SOTA}$	95% CI	$E(\max_j \theta_j)$	# teams
no mult.	$\hat{\theta}^{\max}$	(0.9067,0.9162)	-	-
Kaggle accuracies	$\hat{\theta}^{\max}$	(0.9128,0.9191)	0.9159	-
cropping	0.9062	(0.9084,0.9148)	$\hat{\theta}^{\max}$	1134
	0.9026	(0.9050, $\hat{\theta}^{\max}$)	0.9083	1844

Table 3: The 95% CI and the expectation and for the SOTA estimator for different estimation strategies. The bootstrap standard deviations are in the order of magnitude 10^{-5} - 10^{-4} , and are therefore not displayed.

5.1.2 Cassava Leaf Disease

In this example, the highest reported accuracy is unlikely to be the product of multiplicity. For The Cassava Leaf Disease Classification competition, the task was to classify images of cassava leaves. The training set consisted of 21,367 labelled images of 5 classes, and the test set of approximately 15,000 images. 3,752 teams participated (excluding those with accuracy lower than chance).

The three top performances appear as outliers, as seen in Figure 8a. The 95% CI of $\hat{\theta}^{\max} = 0.9132$ is (0.9086, 0.9177), no other observations are within this interval. By performing simulations without cropping, we get $E(\hat{\theta}^{\max}) = \hat{\theta}^{\max}$, and although the upper tail is stretched, its tip does not surpass $\hat{\theta}^{\max}$.



(a) The Kaggle performances

(b) One realisation.

Figure 8: The competition observations and one realisation.

Several explanations for the outlying performances of the three top teams have been put forward, and the interested reader can take a deep-dive in the comment section of the competition. Since this is not the topic of the present work, we will not engage in the discussion here.

5.2 Simulation of AUCs

We discuss here an example, the SIIM-ISIC Melanoma Classification competition from 2020 because it follows many of the common structures of public challenges. The winning team chose many of the verified strategies from Section 2.

The SIIM-ISIC Melanoma Classification competition consisted of more than 40,000 images of skin lesions from various sites, split into training (33,126), validation (3,295) and test set (7,687). The data set is highly imbalanced, with less than 2% melanomas, which reflects the reality in many cancer detection situations. A full description can be found in Rotemberg et al. [2021]. The size of the test set is smaller than the recommendations of, e.g., Roelofs et al. [2019], but reflects the reality of benchmark datasets and public challenges, as seen, e.g., in the overview of Willemink et al. [2020]. We want to emphasise that the shortcomings of this competition are not unique, and that is precisely why it serves as a useful example. Participants were allowed to use additional data for training if the data was shared on the competition web site. The prize money was set to 10,000 USD for the best-performing method, measured as AUC on the hold-out test set, published in the private leaderboard as seen in Figure 9. Participants could get intermediate results from the validation set, published on a public leaderboard.

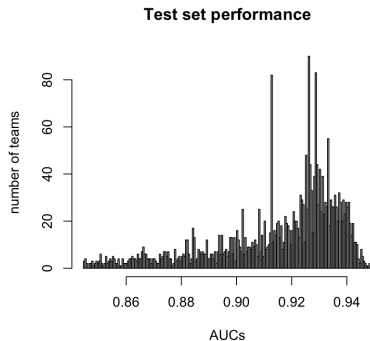


Figure 9: Histogram of the AUCs from the kaggle leaderboard, test set.

The team ‘All Data Are Ext’ consisting of three Kaggle Grandmasters won the competition, achieving an AUC of 0.9490 on the test set, and their method and strategy is explained in Ha et al. [2020]. Although we show that the AUC is an optimistic estimate for the melanoma detection state-of-the-art, we do not question their rank in the challenge. Quite the contrary; the research in Section 2 supports their strategies. They had a low rank on the public leaderboard (880th out of 3300). Their AUC decreased from the public to the private leaderboard, but it was still within the confidence interval. They used additional data from previous years’ competitions, and they also did data augmentation. They chose ensemble learning as a strategy to avoid overfitting, a strategy implicitly

supported by Talagrand [1996]. They also trained on multiple classes, a strategy that Feldman et al. [2019] showed will slow down the overfitting.

In a binary classification problem, the calculation of AUC is based on scores of random variables from the positive and the negative class. The score function plus a threshold is the classifier. The AUC is mathematically equivalent to the probability that a random variable from the positive class will be ranked higher, in terms of score, than a random variable from the negative class [Hanley and McNeil, 1982].

Let $score(\cdot)$ be a function that assigns a score to a random variable. Let $S_+ = score(W_+)$, where W_+ comes from the positive class, and $S_- = score(W_-)$, where W_- comes from the negative class. Then $AUC = P(S_- < S_+) = P(S_- - S_+ < 0)$, which is equivalent to the cdf at value 0. Hence to simulate classifier scores according to a given true or expected AUC, a , we simply need to specify distributions for the variables S_-, S_+ such a way that $P(S_Y - S_X < 0) = a$.

This is particularly simple with Normal distributions, since linear combinations of Normal distributions yields another Normal. Let S_+ and S_- have the distributions

$$S_+ \sim \mathcal{N}(\mu_+, \sigma_+^2) \quad (13)$$

$$S_- \sim \mathcal{N}(\mu_-, \sigma_-^2), \quad (14)$$

where $\mathcal{N}(\mu, \sigma)$ is the Normal distribution with mean μ and variance σ^2 . We then have that

$$AUC = \Phi \left(\frac{0 - (\mu_- - \mu_+)}{\sqrt{\sigma_-^2 + \sigma_+^2}} \right), \quad (15)$$

by linear combination of two Normal distributions, where Φ is the cdf of the standard Normal distribution. Specifying any three of the four parameters above decides the last one for a chosen AUC = a . Figure 10a shows an example where AUC = 0.90.

The distribution of classifier scores, S , is a mixture distribution of the S_+ and the S_- distributions, where the weights, π and $1 - \pi$, correspond to the probability of selecting a positive or a negative random sample, and has pdf

$$\pi f_+(s) + (1 - \pi)f_-(s), \quad (16)$$

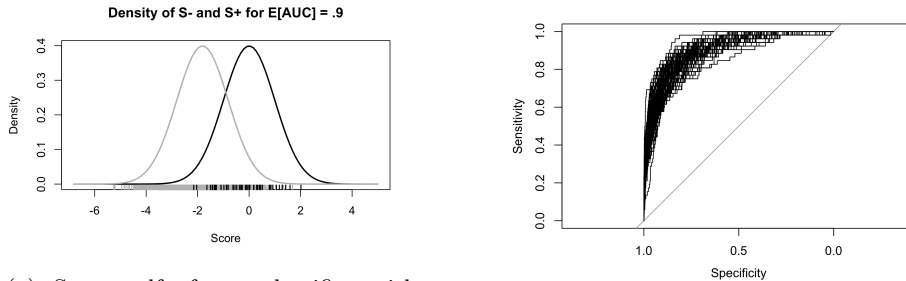
where $f_+(s)$ and $f_-(s)$ are the pdfs of the positive and the negative class, respectively. Expected value and variance of S are

$$\mu = \pi\mu_+ + (1 - \pi)\mu_-, \text{ and} \quad (17)$$

$$\sigma^2 = \pi(\sigma_+^2 + \mu_+^2) + (1 - \pi)(\sigma_-^2 + \mu_-^2) - \mu^2. \quad (18)$$

The uncertainty of AUC can be calculated through bootstrapping, but without access to the predictions for each data point in the test set, the analyst must make some assumptions about the shape of the ROC curve.

Figure 10a shows the pdfs of negative and positive scores with an AUC of 0.90. The rug shows an example draw with 3000 images, with the probability of drawing a positive image is 0.017, corresponding to the class balance in the Melanoma challenge. Fig. 10 shows different shapes of ROC curves.



(a) Score pdfs for a classifier with $AUC = 0.90$; grey for negatives, black for positives. The rug shows an example draw from these.

(b) ROC curves for a classifier with expected AUC of 0.90 across 100 realisations of (a).

Figure 10: Example of what an AUC of 0.90 might look like in practice. The right figure shows 100 realizations of a ROC curve from a competition with 3000. Out of the 3000 images, 52 are positives, reflecting the proportion of the Kaggle melanoma challenge. The left figure shows the underlying score distributions that generated the curves of Figure 10b.

However, with high AUC, the shape has less impact, and the analyst’s choices are not suggestive of the overall conclusion.

5.2.1 Simulation results for uncorrelated classifiers

For simplicity we choose $\mu_- = 0$ and $\sigma_- = \sigma_+ = 1$. We then solve for μ_+ numerically. Now we can generate scores from the two resulting normal distributions.

To demonstrate the impact that multiplicity can have in a public competition, we start with a simulated example similar to the one in Section 3.4. Consider a classification problem with a test set of size $n = 3,000$, number of participating teams, $m = 1,000$, where each classifier has a true underlying AUC of $a = 0.90$, and the classifiers are independent.

Whereas the distribution of $\hat{\theta}^{\max}$ is independent of the class balance as long as the probability of correct prediction is independent of class, this is not true for maximum of \hat{AUC} , where the variance increases with class imbalance. We have chosen the same class balance as in the Melanoma challenge, as this reflects real world examples. The 95% CI of a single classifier with observed AUC equal to its true AUC of 0.90 is $(.8558, 0.9376)$, and gives a strong indication of what we can expect when 1,000 teams apply their classifiers on a test set.

Figure 11 shows the simulated distribution of the observed maximum AUC over 10,000 repetitions of a competition where every classifier has a true AUC of

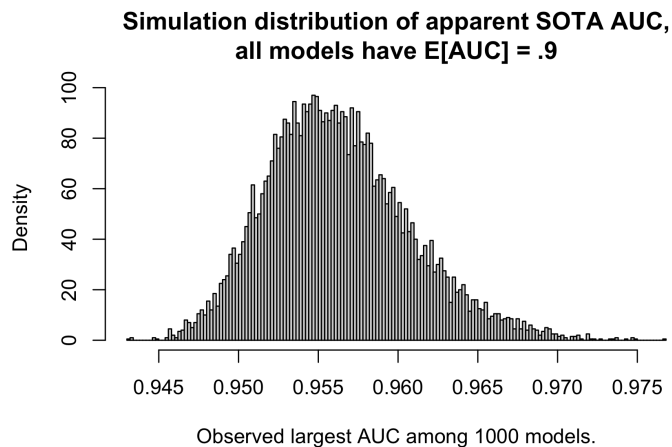
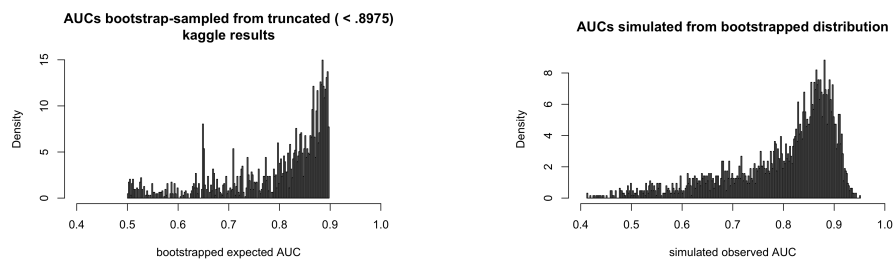


Figure 11: Example distribution of simulated observed state of the art with parameters as in Figure 10. This is an analogous figure to Figure 3 above.

0.90. The simulated expected value is 0.9562, the standard deviation is 0.004459, and the simulated 95% CI is (0.9486, 0.9662).

To give an unbiased estimate of the SOTA performance for the Melanoma challenge, we follow the same procedure as in Section 5.1: The competition observations are cropped in such a manner that their realisations give an expected value of 0.9490, the observed maximum.



(a) One bootstrap sample from the cropped distribution.

(b) One realisation of the bootstrap sample in (a).

Figure 12: Histogram of cropped competition observations. Here the state of the art is an AUC of 0.8975 which leads to the expected observed maximum AUC in a competition being 0.9490.

Figure 12a shows one bootstrap sample from the kaggle observations cropped at 0.8975. Number of classifiers is set to $m = 3,173$, which is as many as there are classifiers in the melanoma challenge with $AUC > 0.5$. Figure 12b shows a

corresponding realisation, where the expected maximum is 0.9490.

There are 2022 teams with performance above the new SOTA candidate.

5.2.2 Correlation between classifiers in the AUC simulations

For the moment we have not extended our AUC simulations to include correlations, but it should be possible to adopt a similar setup as in Sections 4.1 and 4.3: each classifier produces scores that correlate to those of a reference classifier. Let S_{0+} and S_{0-} be the scores of the reference classifier, for random variables from the positive and negative class, respectively.

Let $\rho_+ = \text{corr}(S_{0+}, S_{j+})$ be the correlation between the reference classifier scores S_{0+} and the scores of classifier j , S_{j+} for the positive class. If they both follow Normal distributions as outlined above, then the bivariate distribution is

$$\begin{pmatrix} S_{0+} \\ S_{j+} \end{pmatrix} \sim \mathcal{N} \left(\begin{pmatrix} \mu_{0+} \\ \mu_{j+} \end{pmatrix}, \begin{pmatrix} \sigma_{0+}^2 & \rho\sigma_{0+}\sigma_{j+} \\ \rho\sigma_{0+}\sigma_{j+} & \sigma_{j+}^2 \end{pmatrix} \right),$$

and equivalently for the negative class. However, the joint distribution of (S_0, S_j) is not uniquely defined by the correlation, and simulations are not straightforward.

6 Discussion

We have addressed the mechanisms of multiplicity and how they affect the bias of the SOTA estimator. When accuracy is used as a performance measure, the exact probability distribution can be provided, and known analyses methods can be engaged. The bias in SOTA is substantial in our example, and possibly hinders new methods to attract interest from the scientific community. We have also demonstrated that dependency might not have a big impact on the bias when the probability of correct prediction is already high. The exception is when the dependency is very strong.

We have presented the simple case with an analytical solution, where the probabilities of correct prediction are known.

We have also presented three case-studies from Kaggle competitions, where we demonstrate how a different SOTA candidate than the observed maximum can be estimated, and how it impacts the perceived results.

This work shows that a multiplicity-adjusted state-of-the-art estimate can be calculated fairly easily through bootstrapping, and can serve as a better reference point when introducing new methods to the scientific community.

References

John W Tukey. The philosophy of multiple comparisons. *Statistical Science*, 6: 100–116, 1991. URL https://www.jstor.org/stable/2245714#metadata_info_tab_contents.

- Craig M Bennett, Abigail A Baird, Michael B Miller, and George L Wolford. Neural correlates of interspecies perspective taking in the post-mortem atlantic salmon: An argument for multiple comparisons correction. *Neuroimage*, 47:S125, 2009.
- Janez Demšar. Statistical comparisons of classifiers over multiple data sets. *Journal of Machine Learning Research*, 7:1–30, 2006.
- Steven L. Salzberg. On comparing classifiers: Pitfalls to avoid and a recommended approach. *Data Mining and Knowledge Discovery*, 1:317–328, 1997. ISSN 13845810. doi: 10.1023/A:1009752403260/METRICS. URL <https://link.springer.com/article/10.1023/A:1009752403260>.
- William Hedley Thompson, Jessey Wright, Patrick G. Bissett, and Russell A. Poldrack. Dataset decay and the problem of sequential analyses on open datasets. *eLife*, 9:1–17, 5 2020. ISSN 2050084X. doi: 10.7554/ELIFE.53498.
- Damien Teney, Ehsan Abbasnejad, Kushal Kafle, Robik Shrestha, Christopher Kanan, and Anton van den Hengel. On the value of out-of-distribution testing: An example of goodhart’s law. *Advances in Neural Information Processing Systems*, 33:407–417, 2020.
- Antonio Torralba and Alexei A. Efros. Unbiased look at dataset bias. *Proceedings of the IEEE Computer Society Conference on Computer Vision and Pattern Recognition*, pages 1521–1528, 2011. ISSN 10636919. doi: 10.1109/CVPR.2011.5995347.
- Mark Everingham, S. M.Ali Eslami, Luc Van Gool, Christopher K.I. Williams, John Winn, and Andrew Zisserman. The pascal visual object classes challenge: A retrospective. *International Journal of Computer Vision*, 111:98–136, 1 2015. ISSN 15731405. doi: 10.1007/S11263-014-0733-5/FIGURES/27. URL <https://link.springer.com/article/10.1007/s11263-014-0733-5>.
- Manuel Fernández-Delgado, Eva Cernadas, Senén Barro, Dinani Amorim, and Amorim Fernández-Delgado. Do we need hundreds of classifiers to solve real world classification problems? *Journal of Machine Learning Research*, 15:3133–3181, 2014. URL <http://www.mathworks.es/products/neural-network>.
- Avrim Blum and Moritz Hardt. The ladder: A reliable leaderboard for machine learning competitions. pages 1006–1014. PMLR, 6 2015. URL <https://proceedings.mlr.press/v37/blum15.html>.
- Cynthia Dwork, Vitaly Feldman, Moritz Hardt, Toniann Pitassi, Omer Reingold, and Aaron Roth. Guilt-free data reuse. *Communications of the ACM*, 60:86–93, 4 2017. ISSN 15577317. doi: 10.1145/3051088.

- Benjamin Recht, Rebecca Roelofs, Ludwig Schmidt, and Vaishaal Shankar. Do imagenet classifiers generalize to imagenet? pages 5389–5400. PMLR, 5 2019. URL <https://proceedings.mlr.press/v97/recht19a.html>.
- Vitaly Feldman, Roy Frostig, and Moritz Hardt. The advantages of multiple classes for reducing overfitting from test set reuse. pages 1892–1900. PMLR, 5 2019. URL <https://proceedings.mlr.press/v97/feldman19a.html>.
- Horia Mania, John Miller, Ludwig Schmidt, Moritz Hardt, and Benjamin Recht. Model similarity mitigates test set overuse. *Advances in Neural Information Processing Systems*, 32, 2019.
- Rebecca Roelofs, Vaishaal Shankar, Benjamin Recht, Sara Fridovich-Keil, Moritz Hardt, John Miller, and Ludwig Schmidt. A meta-analysis of overfitting in machine learning. *Advances in Neural Information Processing Systems*, 32, 2019. URL <https://www.kaggle.com/kaggle/meta-kaggle>.
- Thomas G. Dietterich. Approximate statistical tests for comparing supervised classification learning algorithms. *Neural Computation*, 10:1895–1923, 10 1998. ISSN 0899-7667. doi: 10.1162/089976698300017197. URL <https://direct.mit.edu/neco/article/10/7/1895/6224/Approximate-Statistical-Tests-for-Comparing>.
- Odd Erik Gundersen and Sigbjørn Kjensmo. State of the art: Reproducibility in artificial intelligence. *Proceedings of the AAAI Conference on Artificial Intelligence*, 32:1644–1651, 4 2018. ISSN 2374-3468. doi: 10.1609/AAAI.V32I1.11503. URL <https://ojs.aaai.org/index.php/AAAI/article/view/11503>.
- Zhiyi Ma, Kawin, Ethayarajh, Tristan Thrush, Somya Jain, Ledell Wu, Robin Jia, Christopher Potts, Adina Williams, and Douwe Kiela. Dynaboard: An evaluation-as-a-service platform for holistic next-generation benchmarking. *Advances in Neural Information Processing Systems*, 34:10351–10367, 12 2021. URL <https://eval.ai>.
- Xavier Bouthillier, Pierre Delaunay, Mirko Bronzi, Assya Trofimov, Brennan Nichyporuk, Justin Szeto, Nazanin Mohammadi Sepahvand, Edward Raff, Kanika Madan, Vikram Voleti, Samira Ebrahimi Kahou, Vincent Michalski, Tal Arbel, Chris Pal, Gael Varoquaux, and Pascal Vincent. Accounting for variance in machine learning benchmarks. *Proceedings of Machine Learning and Systems*, 3:747–769, 3 2021.
- Olivier Bousquet and André Elisseeff. Stability and generalization. *Journal of Machine Learning Research*, 2:499–526, 2002. URL <http://sensitivity-analysis.jrc.cec.eu.int/>.
- Michel Talagrand. A new look at independence. *The Annals of Probability*, 24:1–34, 1996. URL https://www.jstor.org/stable/2244830#metadata_info_tab_contents.

- Gaël Varoquaux and Veronika Cheplygina. Machine learning for medical imaging: methodological failures and recommendations for the future. *npj Digital Medicine* 2022 5:1, 5:1–8, 4 2022. ISSN 2398-6352. doi: 10.1038/s41746-022-00592-y. URL <https://www.nature.com/articles/s41746-022-00592-y>.
- Philip J. Boland, Frank Proschan, and Y. L. Tong. Modelling dependence in simple and indirect majority systems. *Journal of Applied Probability*, 26:81–88, 3 1989. ISSN 0021-9002. doi: 10.2307/3214318. URL <https://www.cambridge.org/core/journals/journal-of-applied-probability/article/abs/modelling-dependence-in-simple-and-indirect-majority-systems/070D6335BDDDDC7AF4D70BC9B21B0B7B>.
- Daniel W. Ladd. An algorithm for the binomial distribution with dependent trials. *Journal of the American Statistical Association*, 70:333–340, 1975. ISSN 1537274X. doi: 10.1080/01621459.1975.10479867.
- Masato Hisakado, Kenji Kitsukawa, and Shintaro Mori. Correlated binomial models and correlation structures. *J. Phys. A: Math. Gen.*, 2006.
- Y. H. Wang. On the number of successes in independent trials. *Statistica Sinica*, 3:295–312, 1993.
- Veronica Rotemberg, Nicholas Kurtansky, Brigid Betz-Stablein, Liam Caffery, Emmanouil Chousakos, Noel Codella, Marc Combalia, Stephen Dusza, Pascale Guitera, David Gutman, Allan Halpern, Brian Helba, Harald Kittler, Kivanc Kose, Steve Langer, Konstantinos Lioprys, Josep Malvehy, Shenara Musthaq, Jabpani Nanda, Ofer Reiter, George Shih, Alexander Stratigos, Philipp Tschandl, Jochen Weber, and H. Peter Soyer. A patient-centric dataset of images and metadata for identifying melanomas using clinical context. *Scientific Data* 2021 8:1, 8:1–8, 1 2021. ISSN 2052-4463. doi: 10.1038/s41597-021-00815-z. URL <https://www.nature.com/articles/s41597-021-00815-z>.
- Martin J. Willeminck, Wojciech A. Koszek, Cailin Hardell, Jie Wu, Dominik Fleischmann, Hugh Harvey, Les R. Folio, Ronald M. Summers, Daniel L. Rubin, and Matthew P. Lungren. Preparing medical imaging data for machine learning. *Radiology*, 295:4–15, 2 2020. ISSN 15271315. doi: 10.1148/RADIOL.2020192224/ASSET/IMAGES/LARGE/RADIOL.2020192224.FIG5B.JPEG. URL <https://pubs.rsna.org/doi/10.1148/radiol.2020192224>.
- Qishen Ha, Bo Liu, and Fuxu Liu. Identifying melanoma images using efficientnet ensemble: Winning solution to the siim-isic melanoma classification challenge. 10 2020. doi: 10.48550/arxiv.2010.05351. URL <https://arxiv.org/abs/2010.05351v1>.

J A Hanley and B J McNeil. The meaning and use of the area under a receiver operating characteristic (roc) curve. *Radiology*, 143(1):29–36, Apr 1982. ISSN 0033-8419 (Print); 0033-8419 (Linking). doi: 10.1148/radiology.143.1.7063747.